Heliyon 10 (2024) e26000

Contents lists available at ScienceDirect

Heliyon

journal homepage: www.cell.com/heliyon

Research article

Design of a two-degree-of-freedom magnetic levitation vibration energy harvester for bridge vibration response analysis

Dongming Xie [a,*], Zhen Zheng [b], Yaoliang Zhu [c]

[a] Jinshan College of Fujian Agriculture and Forestry University, Fuzhou 350000, China
[b] College of Civil Engineering, Fuzhou University, Fuzhou 350000, China
[c] School of Engineering, Fujian Jiangxia University, Fuzhou 350000, China

ARTICLE INFO

Keywords:
Bridge vibration
Energy harvesters
Output power
Magnets

ABSTRACT

For bridges with high automobile traffic, a large amount of vibration is generated daily due to cars driving over imperfectly level roads, and a vibration energy harvester can convert this energy into electrical energy, thus providing energy for devices such as bridge health sensors. However, the traditional single degree of freedom magnetic levitation vibration energy harvester (SMEH) has the disadvantage of low output power, so this research designs an improved dual degree of freedom magnetic levitation vibration energy harvester (DMEH), and a mathematical model of the energy harvester is built for simulation tests and an optimization model based on NSGA-II algorithm is developed for optimizing the structural parameters of the energy harvester. The experimental results show that the maximum total output power of DMEH and SMEH on CSSBB1, CSSBB2 and CSSBB3 are 48.7 mW, 36.8 mW, 25.4 mW and 27.2 mW, 21.5 mW, 14.9 mW, respectively, and the minimum total magnet volumes of both on CSSBB1, CSSBB2 and CSSBB3 are 268 cm^3, 132 cm^3, 219 cm^3, 214 cm^3, 86.2 cm^3, 156 cm^3. Based on the experimental data, it is found that the maximum output power of the optimal solution of DMEH is larger than that of SMEH for the selected simply supported girder bridge project, and the volume of the former is also larger than that of the latter, but the degree of increase can still be adapted to the application environment. The research results have some reference significance for improving the energy harvesting efficiency of bridge vibration energy harvesters.

1. Introduction

With the continuous development and progress of science and technology, various industrial fields have been rapidly developed and promoted, among which bridge construction is an important part of the infrastructure construction business in developing countries. With the continuous construction and renewal of bridges, the health condition and service life of bridges are of great importance to the economic development of society and people's life [1]. However, bridges are often subjected to external disturbances and their own fatigue damage in the process of use, resulting in a series of vibration response problems. Effective identification and utilization of bridge vibration response has become a hot issue in engineering design, management, and maintenance [2,3]. In bridge vibration response analysis, the vibration energy harvester is not only a key indicator for measuring vibration loss and assessing the health status of the carcass structure, but also an important device for bridge structural health monitoring [4,5]. Although the

* Corresponding author.
E-mail address: xie_dongming@outlook.com (D. Xie).

https://doi.org/10.1016/j.heliyon.2024.e26000
Received 20 July 2023; Received in revised form 22 December 2023; Accepted 6 February 2024
Available online 11 February 2024

traditional SMEH can accurately measure vibration signals and energy information, there are certain drawbacks in practical engineering applications [6]. For example, since the collector can only measure vibration data along one direction, its measurement of the multi-directional vibration response of the bridge is poor and it is difficult to obtain accurate vibration response data information. In addition, due to the strong flexible attachment characteristics of SMEH, once it is disturbed by external interference, the collected data will be greatly affected, resulting in inaccurate data. The most critical thing is that the output power of SMEH is low, which cannot meet the requirements of load operation with high power requirements. The above three points are the main problems that exist in traditional bridge vibration energy collectors, and they are also the issues that need to be addressed in this study. In order to address the shortcomings of traditional SMEH, a magnetic levitation vibration energy harvester for bridge vibration response analysis was designed in this study, aiming to improve the efficiency of bridge vibration energy utilization.

2. Related works

As the global population and economic levels grow, the demand for energy is increasing and devices for harvesting additional energy from social behavior, including vibration energy harvesters, are becoming more widely used. Lu et al. investigated an electromagnetic Stewart platform with high static stiffness and low dynamic stiffness to reduce vibration over six degrees of freedom and to rationalize the use of vibration energy. Each strut in the Stewart platform contains a moving electromagnet suspended between two fixed permanent magnets, which are configured so that the magnetic spring has both negative stiffness and soft nonlinearity. And the use of stiffness nonlinearity improves the vibration isolation efficiency. To obtain the frequency response functions of the transmittance and power output in the first main resonance, the authors' team applied a harmonic balance method based on rigid body dynamics and nonlinear elasticity theory, and the energy acquisition structure was designed based on these theories. Both analytical and numerical results show that the vibration isolation band in the case project extends to lower frequencies and produces a considerable power output for vibrational energy conversion [7–10]. Chen et al. found it particularly valuable to develop efficient methods to prepare the required photothermal converters. The authors' team therefore designed a device that converts light energy into mechanical vibrations and thus into electrical energy, based on the bond-stretching vibration-induced photothermal theory. Experimental results show that the energy conversion efficiency of this device for weak light is slightly higher than that of the conventional method [11]. Wang et al. found that vortex vibration wastes a lot of energy, so they designed a device that converts vortex vibration into electrical energy. The test results show that the device can effectively convert the mechanical energy of eddy excitation vibration and has some practical value [12]. Cai Q applied the theory of electronic power and structural dynamics to design an improved vibration energy harvester that can capture both the mechanical energy of vibration and the energy of damping effect. The test results show that this energy harvester has high application value in some capital vibration devices [13]. Ke et al. found that the shape memory alloy hybrid composite obtained by weaving shape memory alloy into composite materials is a more excellent raw material for making vibration energy harvesters. The results of a comparative experiment conducted by the authors' team showed that the vibration energy harvester designed in this study can convert vibration mechanical energy more efficiently and the designed harvester has a lower self-weight than the conventional device [14]. Zhang et al. Although parabolic trough collectors can collect solar energy effectively, wind loads can pose a threat to the proper operation of this device. Although parabolic trough collectors are effective in collecting solar energy, wind loads can pose a threat to the normal operation of such devices, leading to a decrease in the service life of the device, a decrease in the efficiency of the device in converting light energy, etc. The authors' team designed a parabolic trough collector that is more resistant to wind and can convert a portion of the wind load into electricity. The performance test experiments were conducted with several parabolic trough collectors in windy areas. The parabolic solar trough collector designed by the authors' team has an application value as it converts more than 35% of wind energy [15]. Zhu et al. developed a power flow control method containing substructures and applied this method to the software system of the vibration controller device. Simulation experimental results show that the vibration mechanical energy conversion rate of the vibration control device arranged with the power flow control method is 14.6% higher compared to the vibration control device before the improvement [16]. Zhu et al. found that magnetorheological elastomers can reversibly adjust their resonant frequency in real-time to effectively prevent resonance in mechanical systems, and have certain application potential in vibration detection. Therefore, the author proposes a tunable shock absorber based on magnetorheological elastomers. The test results show that compared with traditional electromagnetic coils, the designed tunable shock absorber here has improved energy utilization efficiency by 94.25% and space utilization efficiency by 75%, respectively. This combination of self sensing and vibration reduction systems achieves high energy spatial efficiency, which will make intelligent health monitoring of bridges and other autonomous, intelligent, and long-term engineering tasks possible [17]. Zhang and others have designed a structural health monitoring system for gymnasiums with high seismic fortification requirements. The system introduces convolutional autoencoders to optimize vibration detection performance and adjust the power supply mode of the hardware. The results indicate that the designed system can effectively detect unexpected ground vibrations. And after being deployed to self powered vibration detectors, the continuous working time of the equipment has been effectively extended [18]. Goudarzi H G et al. found that in the case of improper operation of control equipment, there is a problem of poor performance of damping controllers in topology structure power grid vibration detection equipment. Therefore, the author designed a controller that combines adaptive wide area damping and installed it in the power grid vibration detection device. The experimental results show that the vibration detector installed with a new controller has higher detection accuracy in the event of personnel operating errors [19].

In summary, although scholars at home and abroad have conducted extensive research to improve the energy conversion efficiency of energy collectors for vibration, wind energy, and other energy sources, the efficiency of energy generation by the bridge body may be higher than that of vibration energy generated by solar panels and wind power generation equipment due to the frequent movement of vehicles, which also has certain research value. To further improve the efficiency of the bridge vibration energy harvester, this study

is needed.

3. Design of dual-degree-of-freedom magnetic levitation vibration energy harvester for bridge vibration response

3.1. Mathematical model building of energy harvester

From the late 20th century to the early 21st century, with the progress of microelectronics technology and materials science, researchers began to explore how to capture energy from the surrounding environment to meet the energy needs of small devices. The small vibrations of bridges are considered a potential source of energy [20–23]. Early vibration energy collectors were usually based on piezoelectric or electromagnetic principles. These methods can work well at certain frequencies, but their efficiency is relatively low for random, low-frequency bridge vibrations. In order to increase collection efficiency and adapt to a wider frequency range, researchers have started researching vibration energy collectors based on magnetic levitation [24]. The emergence of a single degree of freedom magnetic levitation vibration energy harvester is an important progress. Further optimization: Although single degree of freedom collectors bring new opportunities, there are still challenges, especially in terms of multi-directional and variable frequency vibrations. This prompted previous researchers to develop a dual degree of freedom magnetic levitation vibration energy harvester to better adapt to complex bridge vibration environments.

Now, the first step is to design a bridge vibration energy harvester with two degrees of freedom and magnetic levitation characteristics. Then, based on its structure and abstracted application scenarios, a corresponding mathematical model and a parameter optimization model based on genetic algorithm are designed for the finite element model of vehicle bridge coupling vibration, with the aim of further optimizing the structure of the collector.

Below are the ideas for solving the problem in this study. Single degree of freedom magnetic levitation vibration energy harvester (SMEH) can change the acquisition bandwidth by changing the nonlinear stiffness, but it cannot increase its output power. Therefore, a dual degree of freedom magnetic levitation vibration energy harvester (DMEH) with magnetic levitation characteristics is designed to provide electrical power to bridge detection sensors. However, due to the significant impact of DMEH structural parameters on overall performance, the manual design of structural parameters overly relies on designer experience and has low design efficiency. Therefore, here we attempt to construct another DMEH parameter design model based on intelligent optimization algorithms. The DMEH is based on a single-degree-of-freedom energy harvester of the same type, in which a magnet with poles opposite to those of the upper and lower fixed magnets is added between the upper and lower fixed magnets, and a coil is wrapped around the gap between the adjacent magnets to form a two-degree-of-freedom system consisting of two fixed magnets and a magnetically levitated magnet. The repulsive force between the adjacent magnets in DMEH can be equivalently treated as a magnetic spring, and this equivalent spring has the ability to change the stiffness of the system that the latter does not have compared to the mechanical spring (see Fig. 1).

Then the mathematical model of DMEH is designed. The electromechanical coupling circuit is the core element in the mathematical model of DMEH, and the Lorentz force generated by the coil induced current in the structure consumes the mechanical energy of the magnetic levitation system and converts the consumed energy into electrical energy. Therefore the electromechanical coupling circuit can be extracted and abstracted as Fig. 2.

The vibration displacement of the SMEH levitating magnet M with respect to the bridge base is assumed to be x, and m is the corresponding mass. The four magnets in the DMEH system are M_1, M_2, M_3, and M_4, and their masses are m_1, m_2, m_3, and m_4, respectively. The base at the bottom of the bridge is chosen as the origin to build a right angle coordinate system, then the amplitude and vibration frequency of the base at the bottom of the bridge are y_0 and w respectively, while x_2 and x_3 are the vibration displacement of the magnets M_2 and M_3 relative to the base at the bottom of the bridge. The force analysis of the DMEH system and the application of Newton's second law can be obtained from the equations of motion of M, M_2 and M_3 in SMEH and DMEH, see Eq. (1).

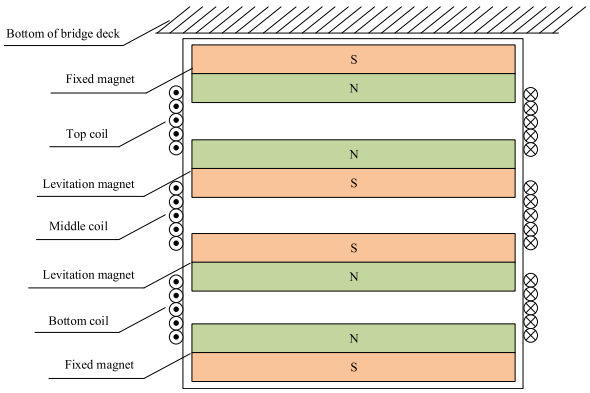

Fig. 1. Schematic diagram of DMEH structure.

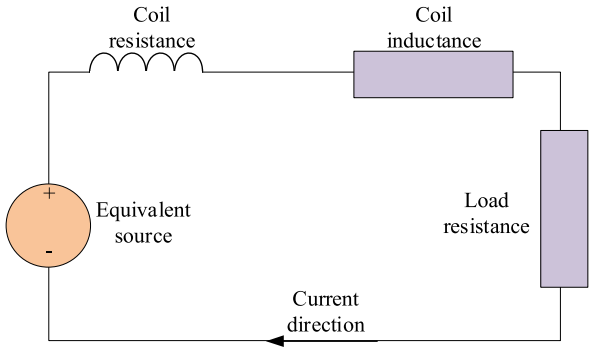

Fig. 2. DMEH electromechanical coupling abstract circuit diagram.

$$\begin{cases} m\ddot{x} = mg - F_r - F_{cv} - F_{ce} - m\ddot{y} \\ m_2\ddot{x}_2 = m_2 g - F_{r2} - F_{cv2} - F_{ce2} - m_2\ddot{y} \\ m_3\ddot{x}_3 = m_3 g - F_{r3} - F_{cv3} - F_{ce3} - m_3\ddot{y} \end{cases} \tag{1}$$

In Eq. (1), F_r, F_{r2}, F_{r3} and F_{cv}, F_{cv2}, F_{cv3} and F_{ce}, F_{ce2} and F_{ce3} represent the repulsive force, viscous damping force and electromagnetic damping force on the corresponding magnets, respectively. According to the first order linear ordinary differential equation initial value problem solving method and the fourth order Runge Kutta method, Eq. (1) problem can be solved. In the same way, the corresponding motion equations $\begin{cases} \ddot{x}_2 = f_2(x_2, x_3, \dot{x}_2, \dot{x}_3) \\ \ddot{x}_3 = f_3(x_2, x_3, \dot{x}_2, \dot{x}_3) \end{cases}$ of M_2 and M_3 can be resolved into the form shown in Eq. (2).

$$\begin{cases} \dot{x}_2 = p_2, \dot{x}_3 = p_3 \\ \dot{p}_2 = g_2(x_2, x_3, p_2, p_3), \dot{p}_3 = g_3(x_2, x_3, p_2, p_3) \\ x_2(0) = 0, x_3(0) = 0 \\ p_2(0) = 0, p_3(0) = 0 \end{cases} \tag{2}$$

In Eq. (2), g_2 and g_3 represent a multivariate function corresponding to the magnet. $\dot{x}_2$, $\dot{x}_3$ and x_2 and x_3 are derived according to the fourth-order Longacurta method, and then $\ddot{x}_2$ and $\ddot{x}_3$ are obtained by substituting the derived variables into Eq. (1). After constructing the mathematical model of DMEH, the output power calculation method of the structure can be deduced, as follows. The instantaneous power transferred from the coil to the external load resistance during the passage of the levitated magnet through the coil under external excitation $P(t)$ can be calculated according to Eq. (3).

$$P(t) = \frac{\alpha^2 R_{load}}{(R_{load} + R_{coil})^2} \sum_{j=1}^{n+1} \left[\left(\dot{x}_{j+1} - \dot{x}_j \right)^2 \right] \tag{3}$$

In Eq. (3), R_{load} and R_{coil} represent the total load resistance and total coil resistance in the equivalent circuit, respectively. j is the magnet number, n is the coil number, and α is the electromechanical coupling coefficient, which is a known parameter related to the materials used to compose the energy harvester. After the external excitation continues until the energy collector operates stably, the external load resistance of the structure corresponds to the average output power of P_m, which can be calculated according to Eq. (4).

$$P_m = \frac{1}{T} \frac{\alpha^2 R_{load}}{(R_{load} + R_{coil})^2} \sum_{t=0}^{n+1} \left[\sum_{j=1}^{n+1} \left(\dot{x}_{j+1} - \dot{x}_j \right)^2 \Delta t \right] \tag{4}$$

In Eq. (4), T is the corresponding time period for calculating the average output power.

3.2. Finite element modeling of axle coupling vibration

After designing the structure and components of DMEH in the previous section, in order to further improve the performance of the object, it is necessary to construct a mathematical model for optimizing the main structural parameters of DMEH. The design of this parameter optimization model needs to consider the practical application scenarios of DMEH. Therefore, it is necessary to first model the bridge vibration mode in the DMEH application scenario. The vehicle load that brings bridge vibration in this study is set to be generated by a common tri-axle truck, because this vehicle type has a good representation. The geometric parameters, tire stiffness and damping system, and mass distribution of the three-axle truck were obtained in accordance with the relevant domestic specifications. In the study, a more common length of 24.60 m prestressed concrete simply supported girder bridge was chosen as the basis for analyzing the vibration response of the bridge. The finite element model of the bridge was designed using the finite element design software Ansys. Taking into account the construction material and operating conditions of the bridge, the 3D solid unit solid 45 was

chosen to simulate the main body of the bridge, and the translational degrees of freedom were set for each node in three directions: length, width and height. The dynamic response in the finite element model is calculated by the modal synthesis method, and considering the calculation accuracy, it is reasonable to carry out the dynamic calculation in accordance with the 20~40th order modal. In order to simplify the vibration law of the bridge coupled vibration model, the driving route of the vehicle is specified to be parallel to the centerline of the bridge, and the cross-section of the bridge with the loading position of the three-axle truck is added as shown in Fig. 3.

The main source of bridge coupling vibration is the impact load generated by vehicles as they pass over uneven pavements. The pavement power spectral density function is generally used in the industry to describe the pavement unevenness. And in the numerical simulation process, the power spectral density function can be used to generate the unevenness of the bridge deck according to the inverse Fourier transform, so Eq. (5) is designed here as the bridge deck roughness measurement model.

$$r(X) = \sum_{k=1}^{N} \sqrt{2\varphi(n_k)\Delta n \cos(2\pi n_k X + \theta_k)} \tag{5}$$

In Eq. (5), $r(X)$ is the bridge deck flatness along the longitudinal axis of the bridge deck at a distance of X, the phase angle θ_k varies in the range of $(0, 2\pi)$, φ is the power spectral density function measuring the roughness of the pavement, n_k is the spatial frequency or travel frequency with inverse relationship to the wavelength, n_k describes the total number of times a harmonic quantity appears in each meter of length, and n is the total number of frequencies distributed according to n_k. Therefore, the corresponding power spectrum function of pavement unevenness can be obtained. Then the axle coupling vibration equation is designed, as shown in Eq. (6).

$$[M_v]\left\{\ddot{d}_v\right\} + [C_v]\{\dot{d}_v\} + [K_v]\{d_v\} = \{F_G\} + \{F_v\} \tag{6}$$

In Eq. (6), $[M_v]$, $[C_v]$, $[K_v]$ represent the matrices of vehicle mass, vehicle damping and tire stiffness, respectively; $\{F_G\}$, $\{d_v\}$ represent the vehicle gravity vector and vehicle displacement vector, respectively; $\{F_v\}$ is the contact force vector on the wheels in contact with the road surface. Referring to Eq. (6), it can be seen that the motion equation of the bridge can be described according to Eq. (7).

$$[M_b]\left\{\ddot{d}_b\right\} + [C_b]\{\dot{d}_b\} + [K_b]\{d_b\} = \{F_b\} \tag{7}$$

In Eq. (7), $[K_b]$, $[C_b]$, and $[M_b]$ represent the stiffness, damping, and mass matrices of the bridge, respectively; $\{d_b\}$ and $\{F_b\}$ represent the displacement matrix and the wheel contact force matrix of the bridge, respectively. The modal superposition method and the fourth-order Longacuata method can be used to solve Eqs. (6) and (7), the calculation process is more common.

3.3. Multi-objective optimization model design of energy harvester based on GA algorithm

The core task of this section is to design a parameter optimization model for DMEH based on the previous research work. Before applying the energy harvester to a practical scenario, the acceleration response amplitude characteristics of the bridge under vehicle action in different operating conditions can be analyzed and the acceleration amplitude ratios of the bridge under different order frequency vibration conditions can be counted for subsequent optimization of the structural parameters of the energy harvester using simple harmonic vibration excitation. The first and third order frequency acceleration amplitude spectra of the bridge $A_{f_{b1}}$ and A_{f3} are set at $\theta = \frac{A_{f_{b1}}}{A_{f3}}$ in the study. According to the bridge in actual operation, the bridge deck leveling level in the working condition is classified as: poor, medium and good, and the vehicle speed is classified as several kinds of 120, 105, 90, 75, 60, 45 and 30 km/h. Due to the varying effects of the height, radius, and spacing parameters of different layers of cylindrical magnets on the output power and total volume of DMEH, the efficiency of manually debugging parameter schemes is extremely low, and the found schemes may differ significantly from the optimal ones. Therefore, an intelligent parameter optimization model is constructed using the GA algorithm. Equation (8) shows the objective function of the optimization model, Eqs. (9) and (10) show the corresponding constraint functions. It

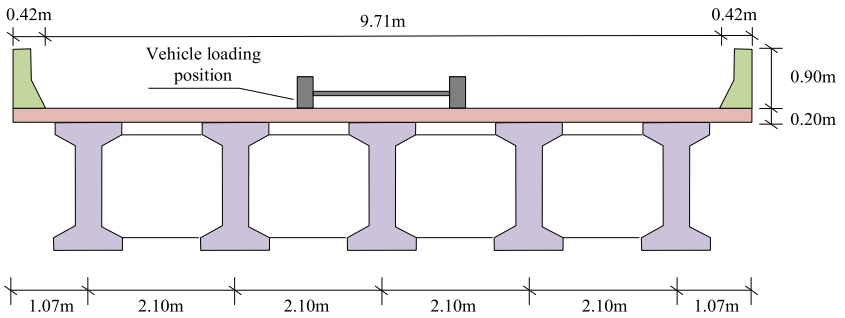

Fig. 3. Cross section of bridge and display of vehicle loading position.

is found that θ obeys the law of log-normal distribution, and the coefficient of determination and the sum of squared residuals are 0.861 and 0.005 respectively. When in simple harmonic vibration motion, the output power corresponding to the excitation frequencies f_{b1} and f_{b3} of the energy harvester are P_1 and P_2 respectively. Then $P_\theta = (\theta P_1 + P_2)$ can be defined to measure the total output power of the energy harvester under the specified condition for different values of θ. $P_{\max}$ It can be seen that P_θ is also log-normally distributed, and the total output power of the bridge under vibration conditions can be calculated from the integration of $f(\theta)P_\theta$ in the interval $[0,\theta_{\max}]$. In order to facilitate computer experiments on these calculation steps, the two objective functions are unified to find the minimum value, so the objective optimization function of the energy harvester can be written as Eq. (8).

$$\begin{cases} P_{\min} = -\alpha P_1 - \beta P_2 \\ V_{\min} = \sum_{i=1}^{4} \left(\pi R_i^2 H_i\right) \end{cases} \tag{8}$$

In Eq. (8), R_i and H_i represent the radius and height of the i magnet respectively, while α and β represent the scale coefficients of P_1 and P_2 respectively. The integration of the probability distribution formula of θ can calculate that α and β are 0.62 and 0.96 respectively. The first constraint is the design variables, i.e., the height, radius and spacing of the four magnets need to meet the range of existing market products; the second constraint is the design domain, i.e., the spatial dimensions of the energy harvester need to meet the requirements of installation and normal operation, so the height, radius and spacing of the four magnets also need to meet the conditions shown in Eq. (9).

$$d \in (0, 120] mm R_i, H_i \in (0, 50] mm \tag{9}$$

Finally, the resonant frequency constraint, because the first order frequency in the bridge vibration, the third order frequency acceleration amplitude half bandwidth size in about 0.2 Hz, so the bridge main vibration frequency and the energy harvester resonant frequency difference cannot be greater than 0.2 Hz, as shown in Eq. (10).

$$\begin{cases} |f_{m1} - f_{b1}| \le 0.2 Hz \\ |f_{m2} - f_{b3}| \le 0.2 Hz \end{cases} \tag{10}$$

The optimization model of the two-degree-of-freedom magnetically levitated vibration energy harvester is thus designed. Then the algorithm for solving this optimization model is selected. Single-objective optimization problems are usually solved by genetic algorithms, but traditional genetic algorithms have many shortcomings in their ability to solve multi-objective optimization problems. Therefore, the Elitist Non-Dominated Sorting Genetic Algorithm (NSGA-II) with elitist strategy is used to carry out the optimization computation. In this algorithm, the complexity of the algorithm is reduced by the fast non-dominated sorting process, and the elitist strategy is introduced to improve the retention probability of good variant individuals, which is shown in Fig. 4. The remaining individuals are eliminated to form the next generation of parental population.

For the problem under study, there are certain mutual constraints between the objective functions $P_{\min}$ and $V_{\min}$, since a decrease in one of the objective values tends to lead to an increase in the other. Therefore, a set of suboptimal solutions needs to be calculated using NSGA-II, from which the one with the highest output power is selected as the final output solution. After considering the solution model and the characteristics of the research problem, a two-degree-of-freedom magnetic levitation vibration energy harvester parameter optimization design solution model based on NSGA-II algorithm is designed, and its computational flow is shown in Fig. 5.

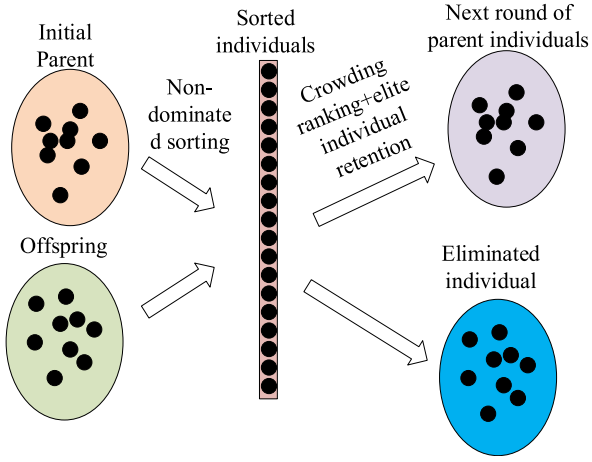

Fig. 4. Elite strategy execution process of NSGA - II algorithm.

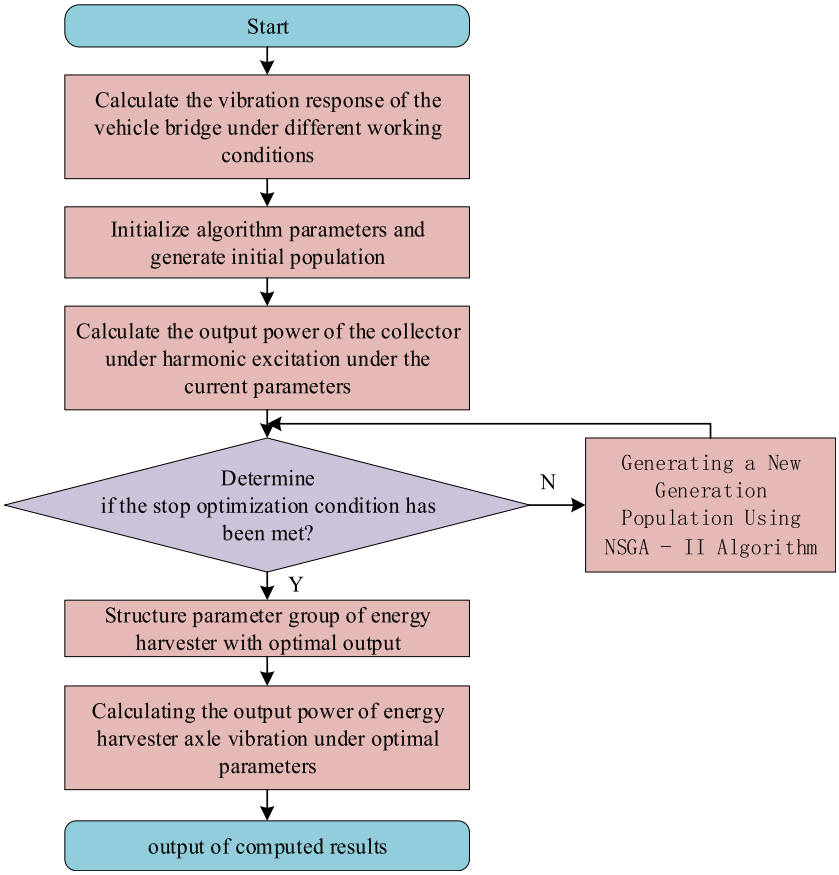

Fig. 5. Calculation process for solving the parameter optimization problem of a dual degree of freedom maglev vibration energy harvester.

4. Optimization design result analysis of dual-degree-of-freedom magnetic levitation vibration energy harvester

Considering that the acceleration range of bridge vibration brought by vehicles is 0.5 m/s^2 -1.5 m/s^2, the excitation amplitude generated by simple harmonic vibration should be set to 1 m/s^2. Combined with the application experience of NSGA-II algorithm in the industry and the characteristics of this axle vibration data, after several debugging, the target parameters, design variables, constraints, population size, number of iteration steps, the crossover coefficient, and the coefficient of variation in NSGA-II algorithm are taken as 2, 9, 2, 100, 200, 0.8, and 0.4, respectively, To increase the comparative value of the study, the SMEH is now used to construct a comparative parameter optimization model according to the same algorithm. The parameters of the SMEH optimization design model are selected in the same way as those of the DMEH. Three concrete simply supported girder bridges of different sizes were selected for the study to assist the optimized design of the vibration energy harvester, and to simplify the description, the abbreviations CSSBB1, CSSBB2, and CSSBB3 were given, and the basic information of the three simply supported girder bridges is shown in Table 1. In addition, each type of simply supported girder bridge.

The mathematical models of NSGA-II algorithm, SMEH and DMEH are written in Python language, and the data of the optimal solution set after the optimization of each model is completed are counted to obtain Fig. 6. Fig. 6(a)–(c) respectively show the Pareto optimal solution set distribution of simply supported beam bridges CSSBB1, CSSBB2, and CSSBB3 using two vibration energy harvesting models: DMEH and SMEH. The horizontal and vertical axes in Fig. 6 show the negative number of the probability in the maximum output and the total volume of the minimum magnet, respectively, and the icons of different colors represent different energy harvester models. Analysis of Fig. 6 shows that after both models have completed the optimization calculation, there is an

Table 1
Basic information of the simple supported beam bridge case used in the research institute.

Referred to as	First order basic frequency (Hz)	Third order basic frequency (Hz)	Second moment of area (10 m)$^{-24}$	Cross sectional area (m)^2	Span (m)	α	β
CSSBB1	4.50	11.24	5.326	0.359	24.47	0.63	0.95
CSSBB2	3.10	11.50	10.862	0.514	31.86	0.65	0.92
CSSBB3	2.60	9.08	31.961	0.748	39.58	0.42	0.55

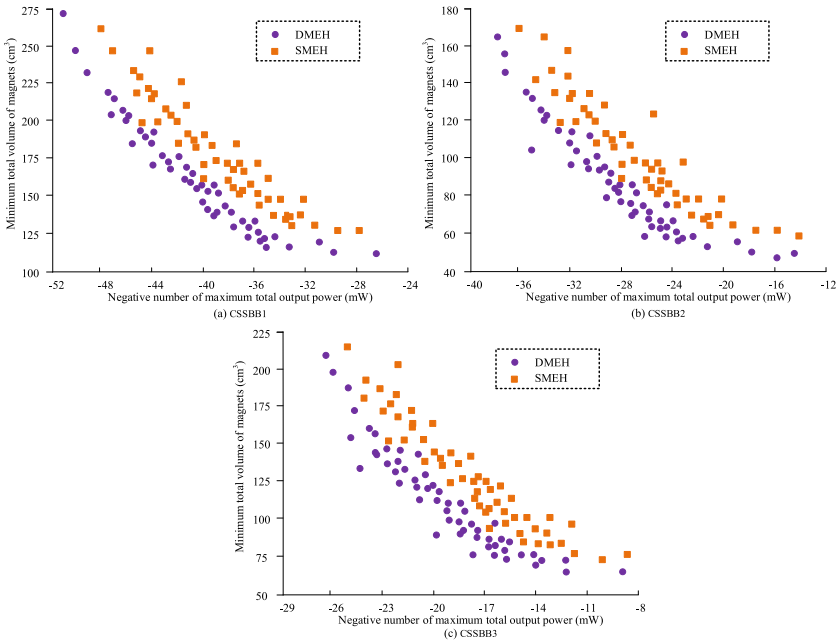

Fig. 6. Pareto optimal solution set display of two models.

overall negative correlation between the negative number of the probability in the maximum output and the total volume of the minimum magnet for the model pareto optimal solution. This conclusion is supported by the fact that the area of the rectangle formed by the perpendicular line with the horizontal and vertical coordinates of the DMEH model data points is smaller than that of the SMEH model, regardless of the simply supported girder bridge, as can be seen from the direct observation on Fig. 6 model.

$P_{\max}$ the optimal solutions were selected from the set of pareto optimal solutions of the two models according to the set rules, and the statistics were obtained in Table 2. $V_{\max}{}^{333333}$ the maximum output power of the optimal solution of DMEH is significantly larger than that of SMEH for all three bridge projects, but the total minimum magnet volume of the former is also larger than that of the latter.

In the following, two energy harvesters are set up with the parameters shown in Table 2, and arranged in the bridge-vehicle coupled vibration model, and the vibration acceleration brought by the vertical direction vehicle driving corresponding to the span position of the bridge is used as the excitation to carry out the simulation experiment. The purpose of the experimental simulation is to simulate the vibration energy harvesting efficiency of the two energy harvesters being followed on the bridge. In order to make the results clearer and more reasonable, the statistics of the total power output of DMEH in different pavement leveling will be counted here according to different pavement leveling, and the statistics of the total power output of DMEH in different pavement leveling are shown in Fig. 7. Fig. 7(a)–(c) depict the total power output of the DMEH energy harvester of simply supported beam bridges CSSBB1, CSSBB2, and CSSBB3 under different road roughness conditions and vehicle driving speed conditions, respectively. The horizontal axis of Fig. 7 represents the form speed of the vehicle in the simulation test, and the vertical axis represents the value of the total power output of DMEH in mW in the corresponding case. Analysis of Fig. 7 shows that for CSSBB1, CSSBB2 and CSSBB3, there is a similar variation relationship between the total power output of the energy harvester and the vehicle driving speed. The total output power of each item starts to increase when the driving speed starts to increase from 30 km/h. When the driving speed exceeds a certain value, the driving

Table 2
Comparison of design parameter values for the optimal solution of two models.

Parameter	DMEH			SMEH		
	CSSBB1	CSSBB2	CSSBB3	CSSBB1	CSSBB2	CSSBB3
$H_1/\ mm$	8	7	29	8	8	8
$H_2/\ mm$	36	14	32	39	17	35
$H_3/\ mm$	25	20	36	26	20	38
$H_4/\ mm$	25	20	8	/	/	/
$R_1/\ mm$	6	6	5	6	7	5
$R_2/\ mm$	27	31	23	28	33	22
$R_3/\ mm$	37	35	33	36	35	35
$R_4/\ mm$	29	14	15	/	/	/
$d/\ mm$	98	96	107	95	97	102
$P_{\max}/\ mW$	48.7	36.8	25.4	27.2	21.5	14.9
$V_{\max}/\ cm^3$	268	132	219	214	86.2	156

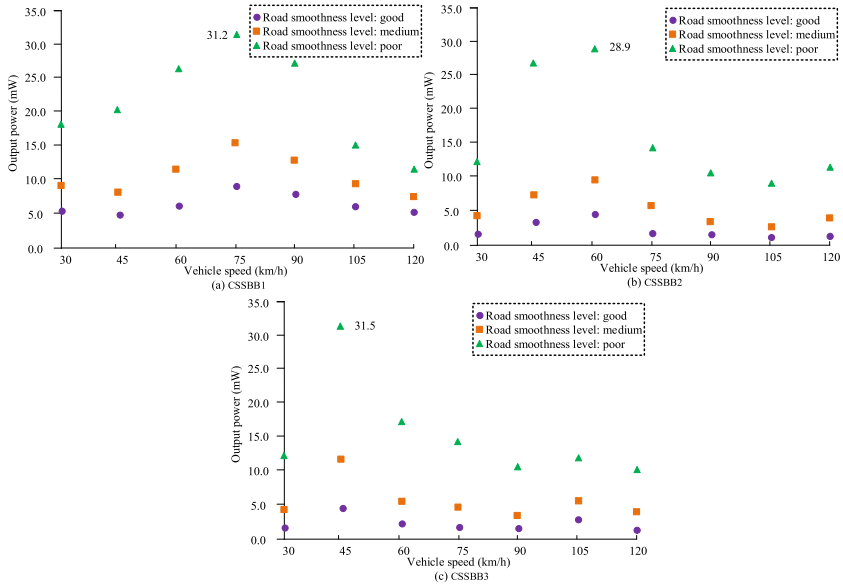

Fig. 7. Comparison of the total output power of DMEH under different road surface roughness conditions.

speed continues to increase and the total output power of each item starts to decrease overall. Specifically, the maximum total output power and corresponding driving speed of DMEH on CSSBB1, CSSBB2 and CSSBB3 are 31.2 mW, 28.9 mW, 31.5 mW with 75 km/h, 60 km/h and 45 km/h. From the perspective of road leveling, the worse the road leveling is, the greater the output power of the collector when other conditions are the same, which This is consistent across the bridge test items.

The statistical results of SMEH output total power data in different pavement leveling are shown in Fig. 8. Fig. 8(a)–(c) depict the total power output of the SMEH energy harvesters of simply supported beam bridges CSSBB1, CSSBB2, and CSSBB3 under different road roughness conditions and vehicle driving speed conditions, respectively. The horizontal axis of Fig. 8 represents the form speed of the car in the simulation test, and the vertical axis represents the SMEH output total power values in mW for the corresponding cases. Analysis of Fig. 8 shows that the maximum total output power of SMEH on CSSBB1, CSSBB2 and CSSBB3 and the corresponding driving speed are 25.8 mW, 20.1 mW, 23.5 mW with 75 km/h, 60 km/h and 45 km/h. And from the perspective of road leveling, the worse the road leveling is and the other conditions are the same, the collector the higher the output power, which is also consistent with the statistical results of DMEH. Comparing the results of Figs. 7 and 8, it can be seen that the total output power of DMEH is higher than that of SMEH under various road leveling conditions, for example, when the road leveling is “poor”, the highest total output power of DMEH is 6.0 mW, 8.8 mW and 8.0 mW higher than that of SMEH, respectively.

Finally, the total output power values of each energy harvester on different road surfaces in Figs. 8 and 7 are counted according to the box plot by ignoring the vehicle driving speed, and are used to compare the total output power distribution under different energy harvester and road level condition, and the statistical results are shown in Fig. 9. The horizontal axis in Fig. 9 is used to show different road leveling levels and energy harvester types, and the vertical axis represents the total output power of the harvester, and Fig. 9 The number to the right of the box line in Fig. 9 is the median value of each box. The median, maximum and minimum values are larger than those of SMEH. The median, maximum and minimum values of the total output power under the conditions of “good", “medium" and “poor" were 4.7 mW, 10.1 mW, 18.5 mW and 2.3 mW, 7.4 mW, 15.4 mW, respectively.

In summary, the DMEH designed in this study has obvious advantages in terms of output power, but correspondingly, the more complex design structure will also bring disadvantages in terms of procurement costs. Observing the current construction industry chain market, it can be seen that standardized DMEH products are generally 10%–80% higher than SMEH products. In terms of spatial cost, when designing a DMEH parameter optimization model based on GA algorithm, the constraint setting process has taken into account the spatial limitations of installing vibration energy collectors on the bridge, so the space cost required for the designed structure is still within the allowable range. The technical cost of this study mainly lies in deploying the designed GA based optimization algorithm to the DMEH production workshop and linking the output results with production. It can be seen that for product manufacturers, the technical cost is almost one-time, and through programming and design, it can be combined with existing production processes to produce improved DMEH products, with controllable production costs. In specific bridge engineering, product cost is also one of the evaluation criteria for considering which vibration energy harvester to choose, and needs to be selected based on specific construction conditions and procurement preferences. When the vibration conditions of bridge structures are complex and not conducive to the generation of vibration energy, DMEH has a more significant advantage compared to SMEH. This is because theoretically, the DMEH structure can enable DMEH to receive more directional and formal vibration energy compared to SMEH, which means the former has stronger vibration reception ability.

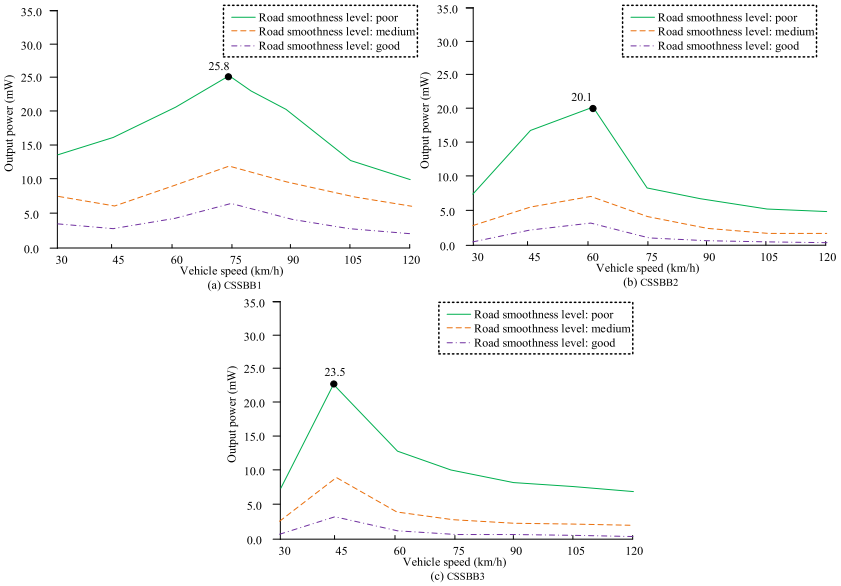

Fig. 8. Comparison of total output power of SMEH under different road surface roughness conditions.

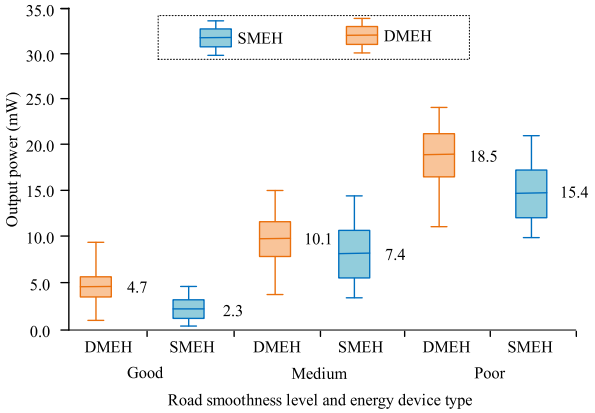

Fig. 9. Output power of two types of energy collectors under different road surface roughness.

5. Conclusion

In order to improve the performance of vibration energy harvester using bridge vibration energy generation, this study designed a dual-degree-of-freedom magnetically levitated vibration energy harvester and designed an energy conversion mathematical model for DMEH, and then used NSGA-II algorithm to optimize the structural parameters of DMEH. The experimental results show that the maximum total output power of DMEH and SMEH on CSSBB1, CSSBB2 and CSSBB3 are 48.7 mW, 36.8 mW, 25.4 mW and 27.2 mW, 21.5 mW, 14.9 mW, respectively, and the minimum total magnet volumes of both on CSSBB1, CSSBB2 and CSSBB3 are 268 cm^3, 132 cm^3, 219 cm^3 and 214 cm^3, 86.2 cm^3, 156 cm^3. The maximum total output power and corresponding driving speed of DMEH on CSSBB1, CSSBB2 and CSSBB3 are 31.2 mW, 28.9 mW, 31.5 mW and 75 km/h, 60 km/h and 45 km/h respectively. SMEH The maximum total output power and corresponding driving speed on CSSBB1, CSSBB2 and CSSBB3 are 25.8 mW, 20.1 mW, 23.5 mW with 75 km/h, 60 km/h, 45 km/h. The total output power of DMEH is greater than SMEH under various road leveling conditions. When the road leveling is “poor", the maximum total output power of DMEH is 6.0 mW, 8.8 mW and 8.0 mW higher than that of SMEH, respectively. On the whole, if ignoring the vehicle driving speed, the variation of total output power of DMEH is larger than that of SMEH, and the median, maximum and minimum values are larger than that of SMEH. Specifically, the median total power output of DMEH and SMEH under the conditions of “good”, “medium” and “poor” road leveling are 4.7 mW, 10.1 mW, 18.5 mW and 10.1 mW, respectively, From the experimental data, it can be seen that the maximum output power of the optimal solution of DMEH is significantly larger than that of SMEH for the selected simply supported girder bridge project, and the volume of the former is larger than that of the latter, but the degree of increase can still be adapted to the application environment. The shortcoming of this study is that more data from different types of bridges were not selected for the experiments, which is an area that needs attention in

subsequent studies.

Funding statement

This work was sponsored in part by Science and Technology Project of Fujian Provincial Department of Education (y160401) and (JAT200996).

Data availability statement

The data used to support the findings of this study are all in the manuscript.

CRediT authorship contribution statement

Dongming Xie: Writing – review & editing, Writing – original draft, Conceptualization. **Zhen Zheng:** Methodology, Formal analysis. **Yaoliang Zhu:** Methodology, Data curation.

Declaration of competing interest

The authors declare that they have no known competing financial interests or personal relationships that could have appeared to influence the work reported in this paper.

References

[1] P. Han, G. Pan, B. Zhang, W. Wang, W. Tian, Three-cylinder oscillator under flow: flow induced vibration and energy harvesting, Ocean Eng. 211 (2020), 107619.1-107619.17.
[2] S. Shaaban, Enhancement of the solar trough collector efficiency by optimizing the reflecting mirror profile, Renew. Energy 176 (2021) 40–49.
[3] M. Zhang, C. Zhang, A. Abdelkefi, H. Yu, O. Gaidai, X. Qin, H. Zhu, J. Wang, Piezoelectric energy harvesting from vortex-induced vibration of a circular cylinder: effect of Reynolds number, Ocean Eng. 235 (2021), 109378.1-109378.13.
[4] C. Liu, R. Zhao, K. Yu, H.P. Lee, B. Liao, A quasi-zero-stiffness device capable of vibration isolation and energy harvesting using piezoelectric buckled beams, Energy 233 (2021), 121146.1-121146.18.
[5] E. Masero, J.M. Maestre, E.F. Camacho, Market-based clustering of model predictive controllers for maximizing collected energy by parabolic-trough solar collector fields, Appl. Energy 306 (2022), 117936.1-117936.12.
[6] X. Liu, C. Sun, Y. Wang, F. Jiang, C. Zhang, Vibration characteristic analysis of transformers influenced by DC bias based on vibration half-wave energy method, Int. J. Electr. Power Energy Syst. 128 (4) (2021), 106725.1-106725.8.
[7] Z.Q. Lu, D. Wu, H. Ding, L.Q. Chen, Vibration isolation and energy harvesting integrated in a Stewart platform with high static and low dynamic stiffness-ScienceDirect, Appl. Math. Model. 89 (Pt. 1) (2021) 249–267.
[8] H. Zhang, X. Xiang, B. Huang, Z. Wu, H. Chen, Static homotopy response analysis of structure with random variables of arbitrary distributions by minimizing stochastic residual error, Comput. Struct. 288 (2023) 107153.
[9] J. Wang, F. Liang, H. Zhou, M. Yang, Q. Wang, Analysis of position, pose and force decoupling characteristics of a 4-ups/1-rps parallel grinding robot, Symmetry 14 (4) (2022) 825.
[10] K. Liao, D. Lu, M. Wang, J. Yang, A low-pass virtual filter for output power smoothing of wind energy conversion systems, IEEE Trans. Ind. Electron. 69 (12) (2022) 12874–12885.
[11] M. Chen, X. Zhang, J. Liu, F. Liu, R. Zhang, P. Wei, H. Feng, M. Tu, A. Qin, W.Y. Lam, D. Ding, B.Z. Tang, Evoking photothermy by capturing intramolecular bond stretching vibration-induced dark-state energy, ACS Nano 14 (4) (2020) 4265–4275.
[12] J. Wang, L. Tang, L. Zhao, G. Hu, R. Song, K. Xu, Equivalent circuit representation of a vortex-induced vibration-based energy harvester using a semi-empirical lumped parameter approach, Int. J. Energy Res. 44 (6) (2020) 4516–4528.
[13] Q. Cai, S. Zhu, The nexus between vibration-based energy harvesting and structural vibration control: a comprehensive review, Renew. Sustain. Energy Rev. 155 (2022), 111920.1-111920.24.
[14] J. Ke, J. Gao, Z.Y. Wu, Z. Xiang, X.D. Hu, Vari-stiffness characteristics of a 3D SMA hybrid basalt woven composite, Compos. Struct. 285 (2022), 115192.1-115192.14.
[15] Z. Zhang, J. Sun, L. Wang, J.J. Wei, Multiphysics-coupled study of wind load effects on optical performance of parabolic trough collector, Sol. Energy 207 (2020) 1078–1087.
[16] C. Zhu, J. Yang, C. Rudd, Vibration transmission and energy flow analysis of L-shaped laminated composite structure based on a substructure method, Thin-Walled Struct. 169 (2021), 108375.1-108375.20.
[17] Z. Zhu, Z. Wang, K. Dai, X.F. Wang, H. Zhang, W.L. Zhang, An adaptive and space-energy efficiency vibration absorber system using a self-sensing and tunable magnetorheological elastomer, Nano Energy 117 (2023) 108927.
[18] M. Zhang, T. Guo, R. Zhu, Y. Zong, Z.X. Liu, W.J. Xu, Damage identification of seismic-isolated structure based on CAE network using vibration monitoring data, Eng. Struct. (2023).
[19] H.G. Goudarzi, B. Yousefi, M. Rezvani, A.N. Shirazi, Adaptive WADC scheme for damping inter-area oscillation based on Jaya optimization algorithm in the presence of variable time latencies from WAMS data, Int. Trans. Electr. Energy Syst. 31 (12) (2021).
[20] W. Hou, Y. Li, Y. Zheng, W. Guo, Multi-frequency energy harvesting method for vehicle induced vibration of rail transit continuous rigid bridges, J. Clean. Prod. 254 (2020), 119981.1-119981.15.
[21] J. Shi, B. Zhao, T. He, L. Tu, X. Lu, H. Xu, Tribology and dynamic characteristics of textured journal-thrust coupled bearing considering thermal and pressure coupled effects, Tribol. Int. 180 (2023) 108292.
[22] Y. Yang, B. Lin, W. Zhang, Experimental and numerical investigation of an arch–beam joint for an arch bridge, Arch. Civ. Mech. Eng. 23 (2) (2023) 101.
[23] C. Guo, J. Hu, Fixed-time stabilization of high-order uncertain nonlinear systems: output feedback control design and settling time analysis, J. Syst. Sci. Complex. (2023), https://doi.org/10.1007/s11424-023-2370-y.
[24] C. Zhang, The active rotary inertia driver system for flutter vibration control of bridges and various promising applications, Sci. China Technol. Sci. (2022), https://doi.org/10.1007/s11431-022-2228-0.